



Largest recent impact craters on Mars: Orbital imaging and surface seismic co-investigation

L. Posiolova, Philippe Lognonné, W. Banerdt, J. Clinton, G. Collins, T. Kawamura, S. Ceylan, I. Daubar, B. Fernando, M. Froment, et al.

► To cite this version:

L. Posiolova, Philippe Lognonné, W. Banerdt, J. Clinton, G. Collins, et al.. Largest recent impact craters on Mars: Orbital imaging and surface seismic co-investigation. *Science*, 2022, 378 (6618), pp.412-417. 10.1126/science.abq7704 . hal-03918132

HAL Id: hal-03918132

<https://hal.science/hal-03918132>

Submitted on 2 Jan 2023

HAL is a multi-disciplinary open access archive for the deposit and dissemination of scientific research documents, whether they are published or not. The documents may come from teaching and research institutions in France or abroad, or from public or private research centers.

L'archive ouverte pluridisciplinaire **HAL**, est destinée au dépôt et à la diffusion de documents scientifiques de niveau recherche, publiés ou non, émanant des établissements d'enseignement et de recherche français ou étrangers, des laboratoires publics ou privés.

Largest recent impact craters on Mars: Orbital imaging and surface seismic co-investigation

Authors: L. V. Posiolova^{1*}, P. Lognonné², W. B. Banerdt³, J. Clinton⁴, G. S. Collins⁵, T. Kawamura², S. Ceylan⁶, I. Daubar⁷, B. Fernando⁸, M. Froment^{2,9}, D. Giardini⁶, M. C. Malin¹, K. Miljković¹⁰, S. C. Stähler⁶, Z. Xu², M. E. Banks¹¹, É. Beucler¹², B. A. Cantor¹, C. Charalambous¹³, N. Dahmen⁶, P. Davis¹⁴, M. Drilleau¹⁵, C. M. Dundas¹⁶, C. Durán⁶, F. Euchner⁶, R. F. Garcia¹⁵, M. Golombek³, A. Horleston¹⁷, C. Keegan¹, A. Khan^{6,18}, D. Kim⁶, C. Larmat⁹, R. Lorenz¹⁹, L. Margerin²⁰, S. Menina², M. Panning³, C. Pardo², C. Perrin¹², W. T. Pike¹³, M. Plasman², A. Rajšić^{10†}, L. Rolland²¹, E. Rougier⁹, G. Speth¹, A. Spiga²², A. Stott¹⁵, D. Susko¹, N. A. Teanby¹⁷, A. Valeh¹, A. Werynski¹, N. Wójcicka⁵, G. Zenhäusern⁶.

Affiliations:

¹Malin Space Science Systems, San Diego, CA, USA.

²Université Paris Cité, Institut de Physique du Globe de Paris, CNRS, Paris, France.

³Jet Propulsion Laboratory, California Institute of Technology, Pasadena, CA, USA.

⁴Swiss Seismological Service, ETH Zurich, Zurich, Switzerland.

⁵Department of Earth Science and Engineering, Imperial College London, London, UK.

⁶Institute of Geophysics, ETH Zurich, Zurich, Switzerland.

⁷Department of Earth, Environmental, and Planetary Sciences, Brown University, Providence, RI, USA.

⁸Department of Earth Sciences, University of Oxford, Oxford, UK.

⁹Earth and Environmental Sciences Division, Los Alamos National Laboratory, Los Alamos, NM, USA.

¹⁰Space Science and Technology Centre, School of Earth and Planetary Sciences, Curtin University, Perth, Australia.

¹¹NASA Goddard Space Flight Center, Greenbelt, MD, USA.

¹²Laboratoire de Planétologie et Géodynamique, UMR6112, Université de Nantes, Université d'Angers, CNRS, Nantes, France.

¹³Department of Electrical and Electronic Engineering, Imperial College London, London, UK.

¹⁴Department of Earth, Planetary and Space Sciences, University of California, Los Angeles, CA, USA.

¹⁵Institut Supérieur de l'Aéronautique et de l'Espace SUPAERO, Toulouse, France.

¹⁶U. S. Geological Survey, Astrogeology Science Center, Flagstaff, AZ, USA.

¹⁷School of Earth Sciences, University of Bristol, Bristol, UK.

¹⁸Physik-Institut, University of Zurich, Zurich, Switzerland.

¹⁹Johns Hopkins Applied Physics Laboratory, Laurel, MD, USA.

²⁰Institut de Recherche en Astrophysique et Planétologie, Université Toulouse III Paul Sabatier, CNRS, CNES, Toulouse, France.

²¹Université Côte d'Azur, Observatoire de la Côte d'Azur, CNRS, IRD, Géoazur, Valbonne, France.

²²Laboratoire de Météorologie Dynamique/IPSL, Sorbonne Université, CNRS, Ecole Normale Supérieure, PSL Research University, Ecole Polytechnique, Paris, France.

†Now at the Department of Earth, Atmospheric, and Planetary Sciences, Purdue University, Lafayette, IN, USA.

*Corresponding author. Email: posiolov@msss.com

This draft manuscript is distributed solely for purposes of scientific peer review. Its content is deliberative and predecisional, so it must not be disclosed or released by reviewers. Because the manuscript has not yet been approved for publication by the U.S. Geological Survey (USGS), it does not represent any official USGS finding or policy.

Abstract: Two 130+ meter diameter impact craters formed on Mars during the later half of 2021. These are the two largest fresh impact craters discovered by the Mars Reconnaissance Orbiter since operations started 16 years ago. The impacts created two of the largest seismic events (magnitudes greater than 4) recorded by InSight during its three-year mission. The combination of orbital imagery and seismic ground motion enables the investigation of subsurface and atmospheric energy partitioning of the impact process on a planet with a thin atmosphere and the first direct test of Martian deep-interior seismic models with known event distances. The impact at 35°N excavated blocks of water ice, which is the lowest latitude ice has been directly observed on Mars.

One-Sentence Summary: Imaging and seismic recordings of meteoritic impacts on Mars help evaluate impact dynamics and deep-interior seismic models.

Main Text:

Seismic recordings of hypervelocity impacts (> 3 km/s) are rare despite being the most common terrain modification process in the solar system. Earth is shielded by its atmosphere, consequently there are few seismically recorded ground impacts, and meteoroids that do reach the ground likely travel at terminal subsonic velocity and only form small craters (1–3). The Apollo Passive Seismic Experiments on the Moon recorded ground motions from artificial impacts, but these had slow relative velocities (< 2.6 km/s) and formed craters smaller than 30 m (4). Larger natural impacts on the Moon were detected but have not been associated with imaged craters (4, 5), and all are expected to be smaller than 100 m in diameter (6). On Earth, a multitude of seismic events with known source locations, e.g. explosion sources, have been used extensively for evaluating seismic velocity models, even down to the Earth's core (7). In contrast, there were only a few confirmed seismic source locations on Mars (all impacts), but these were small (< 12 m in diameter) and near InSight (< 300 km) so the seismic paths only sampled the shallow crust (8). The two new impact craters reported here allow for the first time an evaluation of deep interior Mars global velocity models and an observational investigation of the dynamics of the hypervelocity impact process.

The two major impacts (Fig. 1) were discovered using the Mars Reconnaissance Orbiter's (MRO) Context Camera (CTX) (9) and the Seismic Experiment for Interior Structure (SEIS) (10) of the Interior Exploration on the Seismic Investigations, Geodesy and Heat Transport (InSight) mission (11). Both impacts generated craters > 130 meters in diameter making them the largest fresh craters identified since the beginning of the MRO mission 16 years ago. The seismic events have identifiable surface waves, distinguishing them from other recorded and analyzed events on Mars and indicating shallow sources (12). Before these events, surface waves had not been unambiguously identified on any terrestrial planet other than Earth. The closer impact (ID S1094b) occurred at a distance of 58.5° (3,460 km) from the InSight lander on 24 December 2021 and formed the larger of the two craters (150 ± 10 m in diameter). The other impact (ID S1000a) occurred at a distance of 126° (7,455 km) on 18 September 2021 and formed a cluster of craters (largest 130 ± 12 m in diameter). The formation of the craters was time constrained using the MRO Mars Color Imager (MARCI) (13) to within a day (Table S1) making the association with the seismic events highly probable. The seismic events associated with the impacts have similar characteristics, both with approximately 4.0 magnitudes (Table S1, S2). Because the seismic waves traveled deep in the mantle, both events are critical for analysis of mantle velocity models. However, due to S1000a event's large distance, direct seismic waves are eclipsed by Mars's core (14) and more complex bouncing seismic body wave phases (PP, SS) were detected (Fig. S1). The additional attenuation and scattering experienced by these waves obscures the source characteristics. This makes source analysis much more challenging. In addition, the S1000a associated crater is located on the side of a graben (Fig. S2), which perturbed the blast pattern and prevented an easy identification of impactor parameters. In contrast, the closer impact (S1094b) occurred in a flat, dust covered region. Below, we first analyze the impact process for this closer impact before considering the implications for Mars interior models of both impacts.

One of the remarkable features of the S1094b impact was the prominent surface albedo disturbances it caused allowing for the estimation of ephemeral events that would otherwise be unknown, such as the impactor trajectory and the extent of atmospheric blast waves (Fig. 2, Fig. S3). The bearing of the bolide was estimated to be $60^\circ \pm 5^\circ$ clockwise from north based

on measuring the up-range “forbidden zone” in the albedo ray pattern, and a down-range extended cluster of secondary impacts. We infer that the impactor approached the surface at an elevation angle of approximately 30° from horizontal. A steeper angle requires the asymmetric ejecta pattern to be muted, and a much shallower angle should have led to an elliptical crater planform (15, 16). Two distinct arcuate rays (“scimitars”) extending approximately northwest and south of the impact site likely formed from the superposition of two atmospheric blast waves disturbing surface dust: one generated by the passage of the meteoroid through the atmosphere (Mach cone) and the other by the ground impact (17), thus indicating both blast waves extended to at least 18 km laterally. These arcuate rays provide an independent though consistent measure of the impactor trajectory (56°). The meteoroid struck the surface at 18:49 LMST (Local Mean Solar Time) thus impacting on the orbital trailing side of Mars. We estimate the radial extent of surface dust disturbance from the crater to be 9 km (Fig. S3). This limit is consistent with the atmospheric blast pressure produced by a 0.1-1 kiloton (4×10^{11} - 4×10^{12} J) surface explosive source (Fig. S4). The size of the atmospheric blast allows us to evaluate its contribution to the seismic signal.

Crater size is an important quantity for estimating the kinetic energy and momentum of the impactor for use in numerical models. An image from another camera on MRO, the High Resolution Imaging Science Experiment (HiRISE) (18), revealed more details of the crater and its immediate surroundings (Fig. 2). The crater is irregular in shape with an estimated rim-to-rim diameter of 150 ± 10 meters. The depth of the crater floor to the crater rim based on photogrammetry results using HiRISE stereo images is roughly 21 meters. The abundant craters surrounding the new impact are likely almost all secondaries generated by this primary impactor as in comparison areas far (>10–20 km) from the new impact have few small craters. The bright patches and blocks surrounding the crater reveal that it excavated water ice from the subsurface at a lower latitude (35°N) than any prior ice-exposing crater (39°N) (19).

The geological context from orbital imagery aids in determining the appropriate physical models to use in numerical calculations. The S1094b crater is in the Amazonis Planitia region in an area of rugged volcanic plains (20) with CTX images showing lava-flow morphologies mantled by a modest cover of debris. This indicates that a target ground with properties of porous fractured basalt is appropriate for modeling the surface impact. To account for a harder rock site at the crater compared to the region around InSight, we use a local subsurface velocity model based on terrestrial lava flows (21) extrapolated to Mars surface conditions (22, 23) (Fig. S5; Fig. S6) for seismic modeling.

The seismic source duration for an impact of this size is expected to be shorter than the crater formation timescale and limited to the duration of the non-linear shock wave propagation regime (6). The seismic event, S1094b, has a very broad frequency content and relatively flat spectra, from 0.1 Hz to 3 Hz (Fig. 3) with a signal lasting over 100 minutes (24) due to propagation coda (25). The event has an impulsive first arrival P-wave (1 sec uncertainty), followed by an emergent strong S-wave 6 min later (20 sec uncertainty). The third wave observed, arriving 8 min later, is a Rayleigh surface wave, expressed as a long-period dispersed pulse with 8-15 sec period (12). All body wave phases are characterized by a long coda, indicative of strong scattering due to a near-surface source. The spectra display unusually high corner frequencies (3 Hz) compared to most other seismic events recorded on Mars. Shock physics modeling of the impact in a porous fractured basalt target (Fig. 4) indicates that most of the seismic moment is contained within a few hundred meters of the

impact (orange bar in Fig. 4A). The moment release occurs over a short time period consistent with the cutoff frequency of 3 Hz identified in the P-wave displacement spectrum (Fig. 3D). Above the cutoff frequency, the amplitude shows a cubed frequency dropoff, as also observed for closer, smaller impacts on Mars (8) and for shallow explosions on Earth (26, 27).

Seismic moment (M_0) is the key quantity that links the orbital observations of the impact and the impactor parameters to the seismic observations. For S1094b, the seismic moment estimate from S-body waves was originally calculated assuming a marsquake at 50 ± 30 km depth to be 1.3×10^{15} Nm. (28). However, the impact seismic source deposits its energy at much shallower depths, in the strongly shocked region, estimated to be between 17- and 120-m depth from impact modeling, or approximately 50 m (Fig. 4B). We use our lava-flow seismic velocity model to conclude that the moment of a source at this depth is about 100 times smaller than a corresponding deep-crustal source for the same observed amplitude (Fig. 4A; Fig. S5). This is comparable to the seismic moment estimated from surface wave spectra, $M_0 = 7.5\times10^{13}$ Nm, at the same source depth (Fig. S7).

Empirical and numerical models were used to compute seismic moments for S1094b based on the observed crater size. The imaged crater diameter of 150 ± 10 m corresponds to a vertical impactor momentum of $3.3\pm1.4\times10^9$ Ns based on empirical crater-scaling relationships and impactor mass, angle, and velocity probability distributions (Fig. S8; Fig. S9). For these values, numerical simulations predict seismic moments of $0.5\text{--}1.2\times10^{13}$ Nm for impacts in regolith and $2.8\text{--}7\times10^{13}$ Nm for fractured rock conditions (29, 30). These estimates are consistent with the observed seismic moment corrected for relevant depths in our subsurface model (Fig. 4A). The seismic efficiency was estimated to be 10^{-5} based on scaling relations between seismic moment and crater diameter (31) with an order of magnitude uncertainty. This is lower than values estimated for lunar and Earth analogues (32), but larger than that previously modeled for small martian impact craters (29).

The extensive blast pattern around the S1094b crater suggests some of the seismic energy may also originate from energy released in the atmosphere and then coupled to the ground. Numerical impact simulations suggest that up to 10% of the impact energy is partitioned into kinetic energy on the planetary surface, primarily in the ejecta (33). For impact scenarios on Mars similar to S1094b, simulations with an atmosphere further suggest about 5% of the impact energy is partitioned into the blastwave (34). For an estimated impact energy of $1\text{--}8\times10^{13}$ J (Fig. S4), this could produce an atmospheric blast comparable to a $0.1\text{--}1$ kT ($4\times10^{11}\text{--}4\times10^{12}$ J) surface explosion. Therefore, both seismic and image observations are consistent with such a blast and provide coherent constraints in time and space respectively. Semi-empirical airblast theory (35) extrapolated to Mars suggests such a blast would transition from the strong shock regime after 0.2-0.4 sec, which is consistent with the observed ~ 3 Hz P-wave cut-off frequency. The induced blast pressure is sufficient to mobilize surface dust to a radius of ~ 10 km, which is consistent with the observed disturbed dust pattern (Fig. 1; Fig. S3; Fig. S4). The estimated blast energy translates to an atmospheric moment $M_0 \approx (\gamma-1)E = 0.1\text{--}1.3 \times 10^{12}$ Nm, where γ is the adiabatic index (1.33 for Mars) and E is the blast energy (36). This is remarkably consistent with the moment-depth model when extrapolated to the surface (Fig. 4A), implying that a moment of only 10^{12} Nm released in the atmosphere could explain a substantial part of the seismic body wave signal, with the remaining part coming from direct coupling of the impactor with the ground.

On Earth, atmospheric explosions easily excite surface waves (SW) (37) and are highly sensitive to burst altitude (38). Coupled solid/atmospheric Mars Rayleigh modes (14, 39) are predicted to have excitation coefficients up to 10 times larger for a near-surface atmospheric source compared to one 50 m below the subsurface (Fig. S7). They are expected to have an increase in the excitation coefficients between 0.1 Hz and 0.15 Hz for sources above 50 meter altitude. This is not observed in the estimated S1094b spectra, and may be due to attenuation and scattering, which is not unexpected since scattering effects are predicted to generate increasing attenuation of surface waves with frequency on the Moon and Mars (40). Comparison of S1094b SW spectra with near surface excitation coefficients (Fig. S7) suggests that a portion of the SW signal could have originated from the blast just above the surface.

The Marsquake Service (MQS) (41) using SEIS data (24) estimated the seismic locations for both events (S1094b and S1000a). The distance to the events is determined using S-minus-P arrival times (SS-minus-PP for S1000a) (42, 43) and polarization measurements of P and Rayleigh waves (PP for S1000a) (12). For the closer event (S1094b), the epicentral distance from the InSight lander was estimated to be $59.7^{\circ} \pm 6.1^{\circ}$ ($3,530 \pm 360$ km), as compared to the actual distance of 58.5° (3460 km), a difference of only 70 km. For the second impact, S1000a, the distance was estimated at $128.3^{\circ} \pm 19^{\circ}$ ($7,591 \pm 1240$ km), as compared to the actual distance of 126.1° , a difference of 130 km. Additional source parameters for these events are detailed in Tables S1 and S2.

The close agreement between distance estimates and the imaged locations increases our confidence in the Martian seismic velocity models (44–48) for the regions sampled by the direct body waves (Fig. S10). In particular, the models indicate the absence of mantle discontinuities in the 600 to 700 km depth range, which is the depth at which the P, S, PP, and SS waves turn (44). For the S1000a event, the P_{diff} phase, the P wave that diffracts along the core mantle boundary (CMB), has been tentatively identified (14). The PP- P_{diff} travel time difference is sensitive to lower mantle P-velocities below 800 km. Current models at these depths are constrained by core reflected S phases and the mineral-physics-based V_p/V_s ratio (Fig. S10). The observed PP- P_{diff} does not match the predicted values based on these models. This implies that either the P-velocities at the CMB need adjustment, or the V_p/V_s ratio in the lower mantle is different from current predictions. These two events act as calibrated measurements and help select among various Martian interior seismic velocity models (44–48); they corroborate Mars mantle velocity models to 800 km depth and will help to improve future models down to the CMB.

The first two recorded teleseismic events on Mars with orbital ground-truth observations have been used to constrain Martian interior seismic velocity models and infer dynamic impact processes including seismic moment release, impact source duration, and atmosphere-subsurface energy partitioning. The success in observing the formation of impact craters on Mars using instruments on several missions opens up a more detailed understanding of impact dynamics, atmospheric physics, and the exploration of planetary interiors.

References and Notes

1. W. N. Edwards, D. W. Eaton, P. G. Brown, Seismic observations of meteors: Coupling theory and observations. *Rev. Geophys.* **46** (2008), doi:10.1029/2007RG000253.
2. P. Brown, D. O. ReVelle, E. A. Silber, W. N. Edwards, S. Arrowsmith, L. E. Jackson Jr., G. Tancredi, D. Eaton, Analysis of a crater-forming meteorite impact in Peru. *J. Geophys. Res. Planets.* **113** (2008), doi:10.1029/2008JE003105.
3. E. Gnos, B. A. Hofmann, M. A. Halawani, Y. Tarabulsi, M. Hakeem, M. Al Shanti, N. D. Greber, S. Holm, C. Alwmark, R. C. Greenwood, K. Ramseyer, The Wabar impact craters, Saudi Arabia, revisited. *Meteorit. Planet. Sci.* **48**, 2000–2014 (2013), doi:10.1111/maps.12218.
4. Y. Nakamura, G. V. Latham, H. J. Dorman, Apollo Lunar Seismic Experiment—Final summary. *J. Geophys. Res. Solid Earth.* **87**, A117–A123 (1982), doi:10.1029/JB087iS01p0A117.
5. P. Lognonné, C. L. Johnson, "Planetary Seismology" in *Treatise on Geophysics: Second Edition* (2015), pp. 65–120.
6. T. V. Gudkova, Ph. Lognonné, J. Gagnepain-Beyneix, Large impacts detected by the Apollo seismometers: Impactor mass and source cutoff frequency estimations. *Icarus.* **211**, 1049–1065 (2011), doi:10.1016/j.icarus.2010.10.028.
7. W. Wang, J. E. Vidale, Seismological observation of Earth's oscillating inner core. *Sci. Adv.* **8**, eabm9916 (2022), doi:10.1126/sciadv.abm9916.
8. R. F. Garcia, I. J. Daubar, E. Beucler, L. V. Posiolova, G. S. Collins, P. Lognonné, L. Rolland, Z. Xu, N. Wojcicka, A. Spiga, B. Fernando, G. Speth, L. Martire, A. Rajšić, K. Miljkovic, E. Sansom, C. Charalambous, S. Ceylan, S. Menina, L. Margerin, R. Lapeyre, T. Neidhart, N. A. Teanby, N. C. Schmerr, M. Bonnin, M. Froment, J. F. Clinton, Ö. Karatekin, S. C. Stähler, N. L. Dahmen, C. Duran, A. C. Horleston, T. Kawamura, M. Plasman, G. Zenhäusern, D. Giardini, M. P. Panning, M. C. Malin, W. B. Banerdt, Seismological location and orbital imaging of newly formed craters on Mars. *Nat. Geosci.* **in press** (2022), doi:10.1038/s41561-022-01014-0.
9. M. C. Malin, J. F. Bell III, B. A. Cantor, M. A. Caplinger, W. M. Calvin, R. T. Clancy, K. S. Edgett, L. Edwards, R. M. Haberle, P. B. James, S. W. Lee, M. A. Ravine, P. C. Thomas, M. J. Wolff, Context Camera Investigation on board the Mars Reconnaissance Orbiter. *J. Geophys. Res. Planets.* **112** (2007), doi:10.1029/2006JE002808.
10. P. Lognonné, W. B. Banerdt, D. Giardini, W. T. Pike, U. Christensen, P. Laude, S. de Raucourt, P. Zweifel, S. Calcutt, M. Bierwirth, K. J. Hurst, F. Ijpelaan, J. W. Umland, R. Llorca-Cejudo, S. A. Larson, R. F. Garcia, S. Kedar, B. Knapmeyer-Endrun, D. Mimoun, A. Mocquet, M. P. Panning, R. C. Weber, A. Sylvestre-Baron, G. Pont, N. Verdier, L. Kerjean, L. J. Facto, V. Gharakhanian, J. E. Feldman, T. L. Hoffman, D. B. Klein, K. Klein, N. P. Onufrej, J. Paredes-Garcia, M. P. Petkov, J. R. Willis, S. E. Smrekar, M. Drilleau, T. Gabsi, T. Nebut, O. Robert, S. Tillier, C. Moreau, M. Parise, G. Aveni, S. Ben Charef, Y. Bennour, T. Camus, P. A. Dandonneau, C. Desfoux, B. Lecomte, O. Pot, P. Revuz, D. Mance, J. ten Pierick, N. E. Bowles, C. Charalambous, A. K. Delahunty, J. Hurley, R. Irshad, H. Liu, A. G. Mukherjee, I. M. Standley, A. E. Stott, J. Temple, T. Warren, M. Eberhardt, A. Kramer,

- W. Kühne, E.-P. Miettinen, M. Monecke, C. Aicardi, M. André, J. Baroukh, A. Borrien, A. Bouisset, P. Boutte, K. Brethomé, C. Brysbaert, T. Carlier, M. Deleuze, J. M. Desmarres, D. Dilhan, C. Doucet, D. Faye, N. Faye-Refalo, R. Gonzalez, C. Imbert, C. Larigauderie, E. Locatelli, L. Luno, J.-R. Meyer, F. Mialhe, J. M. Mouret, M. Nonon, Y. Pahn, A. Paillet, P. Pasquier, G. Perez, R. Perez, L. Perrin, B. Pouilloux, A. Rosak, I. Savin de Larclause, J. Sicre, M. Sodki, N. Toulemont, B. Vella, C. Yana, F. Alibay, O. M. Avalos, M. A. Balzer, P. Bhandari, E. Blanco, B. D. Bone, J. C. Bousman, P. Bruneau, F. J. Calef, R. J. Calvet, S. A. D'Agostino, G. de los Santos, R. G. Deen, R. W. Denise, J. Ervin, N. W. Ferraro, H. E. Gengl, F. Grinblat, D. Hernandez, M. Hetzel, M. E. Johnson, L. Khachikyan, J. Y. Lin, S. M. Madzunkov, S. L. Marshall, I. G. Mikellides, E. A. Miller, W. Raff, J. E. Singer, C. M. Sunday, J. F. Villalvazo, M. C. Wallace, D. Banfield, J. A. Rodriguez-Manfredi, C. T. Russell, A. Trebi-Ollennu, J. N. Maki, E. Beucler, M. Böse, C. Bonjour, J. L. Berenguer, S. Ceylan, J. Clinton, V. Conejero, I. Daubar, V. Dehant, P. Delage, F. Euchner, I. Estève, L. Fayon, L. Ferraioli, C. L. Johnson, J. Gagnepain-Beyneix, M. Golombek, A. Khan, T. Kawamura, B. Kenda, P. Labrot, N. Murdoch, C. Pardo, C. Perrin, L. Pou, A. Sauron, D. Savoie, S. Stähler, E. Stutzmann, N. A. Teanby, J. Tromp, M. van Driel, M. Wieczorek, R. Widmer-Schnidrig, J. Wookey, SEIS: Insight's Seismic Experiment for Internal Structure of Mars. *Space Sci. Rev.* **215**, 12 (2019), doi:10.1007/s11214-018-0574-6.
11. W. B. Banerdt, S. E. Smrekar, D. Banfield, D. Giardini, M. Golombek, C. L. Johnson, P. Lognonné, A. Spiga, T. Spohn, C. Perrin, S. C. Stähler, D. Antonangeli, S. Asmar, C. Beghein, N. Bowles, E. Bozdag, P. Chi, U. Christensen, J. Clinton, G. S. Collins, I. Daubar, V. Dehant, M. Drilleau, M. Fillingim, W. Folkner, R. F. Garcia, J. Garvin, J. Grant, M. Grott, J. Grygorczuk, T. Hudson, J. C. E. Irving, G. Kargl, T. Kawamura, S. Kedar, S. King, B. Knapmeyer-Endrun, M. Knapmeyer, M. Lemmon, R. Lorenz, J. N. Maki, L. Margerin, S. M. McLennan, C. Michaut, D. Mimoun, A. Mittelholz, A. Mocquet, P. Morgan, N. T. Mueller, N. Murdoch, S. Nagihara, C. Newman, F. Nimmo, M. Panning, W. T. Pike, A.-C. Plesa, S. Rodriguez, J. A. Rodriguez-Manfredi, C. T. Russell, N. Schmerr, M. Siegler, S. Stanley, E. Stutzmann, N. Teanby, J. Tromp, M. van Driel, N. Warner, R. Weber, M. Wieczorek, Initial results from the InSight mission on Mars. *Nat. Geosci.* **13**, 183–189 (2020), doi:10.1038/s41561-020-0544-y.
 12. D. Kim, W. B. Banerdt, S. Ceylan, D. Giardini, V. Lekic, P. Lognonné, C. Beghein, É. Beucler, S. Carrasco, C. Charalambous, J. Clinton, M. Drilleau, C. Duran, M. P. Golombek, R. Joshi, A. Khan, B. Knapmeyer-Endrun, J. Li, R. Maguire, W. T. Pike, H. Samuel, M. Schimmel, N. Schmerr, S. C. Stähler, É. Stutzmann, M. A. Wieczorek, Z. Xu, A. Batov, E. Bozdag, N. Dahmen, P. M. Davis, T. Gudkova, A. Horleston, Q. Huang, T. Kawamura, S. King, S. M. McLennan, F. Nimmo, M. Plasman, A.-C. Plesa, I. E. Stepanova, E. Weidner, G. Zenhäusern, I. J. Daubar, B. Fernando, R. F. Garcia, L. V. Posiolova, M. P. Panning, Surface waves and crustal structure on Mars. *Science*. **in revision** (2022).
 13. J. F. Bell, M. J. Wolff, M. C. Malin, W. M. Calvin, B. A. Cantor, M. A. Caplinger, R. T. Clancy, K. S. Edgett, L. J. Edwards, J. Fahle, F. Ghaemi, R. M. Haberle, A. Hale, P. B. James, S. W. Lee, T. McConnochie, E. Noe Dobrea, M. A. Ravine, D. Schaeffer, K. D. Supulver, P. C. Thomas, Mars Reconnaissance Orbiter Mars Color Imager (MARCI): Instrument description, calibration, and performance. *J. Geophys. Res. Planets.* **114** (2009), doi:10.1029/2008JE003315.
 14. A. C. Horleston, J. F. Clinton, S. Ceylan, D. Giardini, C. Charalambous, J. C. E. Irving, P. Lognonné, S. C. Stähler, G. Zenhäusern, N. L. Dahmen, C. Duran, T. Kawamura, A. Khan,

- D. Kim, M. Plasman, F. Euchner, C. Beghein, É. Beucler, Q. Huang, M. Knapmeyer, B. Knapmeyer-Endrun, V. Lekić, J. Li, C. Perrin, M. Schimmel, N. C. Schmerr, A. E. Stott, E. Stutzmann, N. A. Teanby, Z. Xu, M. Panning, W. B. Banerdt, The Far Side of Mars: Two Distant Marsquakes Detected by InSight. *Seism. Rec.* **2**, 88–99 (2022), doi:10.1785/0320220007.
15. D. E. Gault, J. A. Wedekind, Experimental studies of oblique impact. *Lunar Planet. Sci. Conf. Proc.* **3**, 3843–3875 (1978).
16. D. Elbeshausen, K. Wünnemann, G. S. Collins, The transition from circular to elliptical impact craters. *J. Geophys. Res. Planets.* **118**, 2295–2309 (2013), doi:10.1002/2013JE004477.
17. B. Ivanov, G. Barnes, I. Daubar, C. Dundas, A. McEwen, J. Melosh, New craters on Mars: Air shock wave traces, 4212 (2020), doi:10.5194/egusphere-egu2020-4212.
18. A. S. McEwen, E. M. Eliason, J. W. Bergstrom, N. T. Bridges, C. J. Hansen, W. A. Delamere, J. A. Grant, V. C. Gulick, K. E. Herkenhoff, L. Keszthelyi, R. L. Kirk, M. T. Mellon, S. W. Squyres, N. Thomas, C. M. Weitz, Mars Reconnaissance Orbiter's High Resolution Imaging Science Experiment (HiRISE). *J. Geophys. Res. Planets.* **112** (2007), doi:10.1029/2005JE002605.
19. C. M. Dundas, M. T. Mellon, S. J. Conway, I. J. Daubar, K. E. Williams, L. Ojha, J. J. Wray, A. M. Bramson, S. Byrne, A. S. McEwen, L. V. Posiolova, G. Speth, D. Viola, M. E. Landis, G. A. Morgan, A. V. Pathare, Widespread Exposures of Extensive Clean Shallow Ice in the Midlatitudes of Mars. *J. Geophys. Res. Planets.* **126**, e2020JE006617 (2021), doi:10.1029/2020JE006617.
20. K. L. Tanaka, J. Skinner Jr, J. Dohm, R. P. III, E. J. Kolb, C. M. Fortezzo, T. Platz, G. G. Michael, T. Hare, Geologic Map of Mars. *Sci. Investig. Map.* **3292** (2014), doi:10.3133/sim3292.
21. P. Lesage, M. J. Heap, A. Kushnir, A generic model for the shallow velocity structure of volcanoes. *J. Volcanol. Geotherm. Res.* **356**, 114–126 (2018), doi:10.1016/j.jvolgeores.2018.03.003.
22. C. Larmat, K. Onodera, R. Maguire, P. Lognonné, Modelling to resolve whether SEIS, the seismometer of the NASA Insight lander, has detected the formation of a 1.5m diameter crater which occurred about 40km away. (2020), doi:10.18715/JGR_NEWCATERMOD_2020.
23. I. J. Daubar, P. Lognonné, N. A. Teanby, G. S. Collins, J. Clinton, S. Stähler, A. Spiga, F. Karakostas, S. Ceylan, M. Malin, A. S. McEwen, R. Maguire, C. Charalambous, K. Onodera, A. Lucas, L. Rolland, J. Vaubaillon, T. Kawamura, M. Böse, A. Horleston, M. van Driel, J. Stevanović, K. Miljković, B. Fernando, Q. Huang, D. Giardini, C. S. Larmat, K. Leng, A. Rajšić, N. Schmerr, N. Wójcicka, T. Pike, J. Wookey, S. Rodriguez, R. Garcia, M. E. Banks, L. Margerin, L. Posiolova, B. Banerdt, A New Crater Near InSight: Implications for Seismic Impact Detectability on Mars. *J. Geophys. Res. Planets.* **125**, e2020JE006382 (2020), doi:10.1029/2020JE006382.
24. InSight Mars SEIS Data Service, SEIS raw data, Insight Mission, IPGP, JPL, CNES, ETHZ, ICL, MPS, ISAE-Supaero, LPG, MFSC. (2019), doi:10.18715/SEIS.INSIGHT.XB_2016.
25. P. Lognonné, W. B. Banerdt, W. T. Pike, D. Giardini, U. Christensen, R. F. Garcia, T.

- Kawamura, S. Kedar, B. Knapmeyer-Endrun, L. Margerin, F. Nimmo, M. Panning, B. Tauzin, J.-R. Scholz, D. Antonangeli, S. Barkaoui, E. Beucler, F. Bissig, N. Brinkman, M. Calvet, S. Ceylan, C. Charalambous, P. Davis, M. van Driel, M. Drilleau, L. Fayon, R. Joshi, B. Kenda, A. Khan, M. Knapmeyer, V. Lekic, J. McClean, D. Mimoun, N. Murdoch, L. Pan, C. Perrin, B. Pinot, L. Pou, S. Menina, S. Rodriguez, C. Schmelzbach, N. Schmerr, D. Sollberger, A. Spiga, S. Stähler, A. Stott, E. Stutzmann, S. Tharimena, R. Widmer-Schnidrig, F. Andersson, V. Ansan, C. Beghein, M. Böse, E. Bozdag, J. Clinton, I. Daubar, P. Delage, N. Fuji, M. Golombek, M. Grott, A. Horleston, K. Hurst, J. Irving, A. Jacob, J. Knollenberg, S. Krasner, C. Krause, R. Lorenz, C. Michaut, R. Myhill, T. Nissen-Meyer, J. ten Pierick, A.-C. Plesa, C. Quantin-Nataf, J. Robertsson, L. Rochas, M. Schimmel, S. Smrekar, T. Spohn, N. Teanby, J. Tromp, J. Vallade, N. Verdier, C. Vrettos, R. Weber, D. Banfield, E. Barrett, M. Bierwirth, S. Calcutt, N. Compaire, C. L. Johnson, D. Mance, F. Euchner, L. Kerjean, G. Mainsant, A. Mocquet, J. A. Rodriguez Manfredi, G. Pont, P. Laudet, T. Nebut, S. de Raucourt, O. Robert, C. T. Russell, A. Sylvestre-Baron, S. Tillier, T. Warren, M. Wieczorek, C. Yana, P. Zweifel, Constraints on the shallow elastic and anelastic structure of Mars from InSight seismic data. *Nat. Geosci.* **13**, 213–220 (2020), doi:10.1038/s41561-020-0536-y.
26. W. R. Walter, K. F. Priestley, "High-Frequency P Wave Spectra from Explosions and Earthquakes" in *Explosion Source Phenomenology* (American Geophysical Union (AGU), 1991; <https://onlinelibrary.wiley.com/doi/abs/10.1029/GM065p0219>), pp. 219–228.
27. S. R. Ford, W. R. Walter, S. D. Ruppert, E. M. Matzel, T. F. Hauk, R. Gok, "Toward an Empirically-Based Parametric Explosion Spectral Model" (LAWRENCE LIVERMORE NATIONAL LAB CA, 2011), (available at <https://apps.dtic.mil/sti/citations/ADA568895>).
28. M. Böse, S. C. Stähler, N. Deichmann, D. Giardini, J. Clinton, P. Lognonné, S. Ceylan, M. van Driel, C. Charalambous, N. Dahmen, A. Horleston, T. Kawamura, A. Khan, M. Knapmeyer, G. Orhand Mainsant, J. Scholz, F. Euchner, W. B. Banerdt, Magnitude Scales for Marsquakes Calibrated from InSight Data. *Bull. Seismol. Soc. Am.* **111**, 3003–3015 (2021), doi:10.1785/0120210045.
29. N. Wójcicka, G. S. Collins, I. D. Bastow, N. A. Teanby, K. Miljković, A. Rajšić, I. Daubar, P. Lognonné, The Seismic Moment and Seismic Efficiency of Small Impacts on Mars. *J. Geophys. Res. Planets.* **125**, e2020JE006540 (2020), doi:10.1029/2020JE006540.
30. A. Rajšić, K. Miljković, G. S. Collins, K. Wünnemann, I. J. Daubar, N. Wójcicka, M. A. Wieczorek, Seismic Efficiency for Simple Crater Formation in the Martian Top Crust Analog. *J. Geophys. Res. Planets.* **126**, e2020JE006662 (2021), doi:10.1029/2020JE006662.
31. N. A. Teanby, J. Wookey, Seismic detection of meteorite impacts on Mars. *Phys. Earth Planet. Inter.* (2011), doi:10.1016/j.pepi.2011.03.004.
32. I. Daubar, P. Lognonné, N. A. Teanby, K. Miljkovic, J. Stevanović, J. Vaubaillon, B. Kenda, T. Kawamura, J. Clinton, A. Lucas, M. Drilleau, C. Yana, G. S. Collins, D. Banfield, M. Golombek, S. Kedar, N. Schmerr, R. Garcia, S. Rodriguez, T. Gudkova, S. May, M. Banks, J. Maki, E. Sansom, F. Karakostas, M. Panning, N. Fuji, J. Wookey, M. van Driel, M. Lemmon, V. Ansan, M. Böse, S. Stähler, H. Kanamori, J. Richardson, S. Smrekar, W. B. Banerdt, Impact-Seismic Investigations of the InSight Mission. *Space Sci. Rev.* **214**, 132 (2018), doi:10.1007/s11214-018-0562-x.
33. J. D. Okeefe, T. J. Ahrens, Impact-induced energy partitioning, melting, and vaporization on terrestrial planets. *Lunar Planet. Sci. Conf. Proc.* **3**, 3357–3374 (1977).

34. I. V. Nemtchinov, V. V. Shuvalov, R. Greeley, Impact-mobilized dust in the Martian atmosphere. *J. Geophys. Res. Planets.* **107**, 17-1-17–8 (2002), doi:10.1029/2001JE001834.
35. S. Glasstone, P. J. Dolan, “The Effects of Nuclear Weapons. Third edition” (Department of Defense, Washington, D.C. (USA); Department of Energy, Washington, D.C. (USA), 1977), p. 662, (available at <https://doi.org/10.2172/6852629>).
36. P. Lognonné, B. Mosser, F. A. Dahlen, Excitation of Jovian Seismic Waves by the Shoemaker-Levy 9 Cometary Impact. *Icarus.* **110**, 180–195 (1994), doi:10.1006/icar.1994.1115.
37. M. N. Toksöz, A. Ben-Menahem, Excitation of seismic surface waves by atmospheric nuclear explosions. *J. Geophys. Res. 1896-1977.* **69**, 1639–1648 (1964), doi:10.1029/JZ069i008p01639.
38. D. G. Harkrider, C. A. Newton, E. A. Flinn, Theoretical Effect of Yield and Burst Height of Atmospheric Explosions on Rayleigh Wave Amplitudes. *Geophys. J. Int.* **36**, 191–225 (1974), doi:10.1111/j.1365-246X.1974.tb03632.x.
39. P. Lognonné, F. Karakostas, L. Rolland, Y. Nishikawa, Modeling of atmospheric-coupled Rayleigh waves on planets with atmosphere: From Earth observation to Mars and Venus perspectives. *J. Acoust. Soc. Am.* **140**, 1447 (2016), doi:10.1121/1.4960788.
40. K. Onodera, T. Kawamura, S. Tanaka, Y. Ishihara, T. Maeda, Numerical Simulation of Lunar Seismic Wave Propagation: Investigation of Subsurface Scattering Properties Near Apollo 12 Landing Site. *J. Geophys. Res. Planets.* **126**, e2020JE006406 (2021), doi:10.1029/2020JE006406.
41. InSight Marsquake Service, Mars Seismic Catalogue, InSight Mission; V9 2022-01-01 (2022), doi:10.12686/A14.
42. M. Böse, J. F. Clinton, S. Ceylan, F. Euchner, M. van Driel, A. Khan, D. Giardini, P. Lognonné, W. B. Banerdt, A probabilistic framework for single-station location of seismicity on Earth and Mars. *Phys. Earth Planet. Inter.* **262**, 48–65 (2017), doi:10.1016/j.pepi.2016.11.003.
43. J. F. Clinton, S. Ceylan, M. van Driel, D. Giardini, S. C. Stähler, M. Böse, C. Charalambous, N. L. Dahmen, A. Horleston, T. Kawamura, A. Khan, G. Orland-Mainsant, J.-R. Scholz, F. Euchner, W. B. Banerdt, P. Lognonné, D. Banfield, E. Beucler, R. F. Garcia, S. Kedar, M. P. Panning, C. Perrin, W. T. Pike, S. E. Smrekar, A. Spiga, A. E. Stott, The Marsquake catalogue from InSight, sols 0–478. *Phys. Earth Planet. Inter.* **310**, 106595 (2021), doi:10.1016/j.pepi.2020.106595.
44. C. Durán, A. Khan, S. Ceylan, G. Zenhäusern, S. Stähler, J. F. Clinton, D. Giardini, Seismology on Mars: An analysis of direct, reflected, and converted seismic body waves with implications for interior structure. *Phys. Earth Planet. Inter.* **325**, 106851 (2022), doi:10.1016/j.pepi.2022.106851.
45. S. C. Stähler, A. Khan, W. B. Banerdt, P. Lognonné, D. Giardini, S. Ceylan, M. Drilleau, A. C. Duran, R. F. Garcia, Q. Huang, D. Kim, V. Lekic, H. Samuel, M. Schimmel, N. Schmerr, D. Sollberger, É. Stutzmann, Z. Xu, D. Antonangeli, C. Charalambous, P. M. Davis, J. C. E. Irving, T. Kawamura, M. Knapmeyer, R. Maguire, A. G. Marusiak, M. P. Panning, C. Perrin, A.-C. Plesa, A. Rivoldini, C. Schmelzbach, G. Zenhäusern, É. Beucler, J. Clinton, N. Dahmen, M. van Driel, T. Gudkova, A. Horleston, W. T. Pike, M. Plasman, S. E. Smrekar,

- Seismic detection of the martian core. *Science*. **373**, 443–448 (2021), doi:10.1126/science.abi7730.
46. A. Khan, S. Ceylan, M. van Driel, D. Giardini, P. Lognonné, H. Samuel, N. C. Schmerr, S. C. Stähler, A. C. Duran, Q. Huang, D. Kim, A. Broquet, C. Charalambous, J. F. Clinton, P. M. Davis, M. Drilleau, F. Karakostas, V. Lekic, S. M. McLennan, R. R. Maguire, C. Michaut, M. P. Panning, W. T. Pike, B. Pinot, M. Plasman, J.-R. Scholz, R. Widmer-Schnidrig, T. Spohn, S. E. Smrekar, W. B. Banerdt, Upper mantle structure of Mars from InSight seismic data. *Science*. **373**, 434–438 (2021), doi:10.1126/science.abf2966.
47. A. Khan, P. A. Sossi, C. Liebske, A. Rivoldini, D. Giardini, Geophysical and cosmochemical evidence for a volatile-rich Mars. *Earth Planet. Sci. Lett.* **578**, 117330 (2022), doi:10.1016/j.epsl.2021.117330.
48. M. Drilleau, H. Samuel, R. F. Garcia, A. Rivoldini, C. Perrin, C. Michaut, M. Wieczorek, B. Tauzin, J. A. D. Connolly, P. Meyer, P. Lognonné, W. B. Banerdt, Marsquake locations and 1-D seismic models for Mars from InSight data (2022), doi:10.1002/essoar.10511074.2.
49. M. C. Malin, K. S. Edgett, Mars Global Surveyor Mars Orbiter Camera: Interplanetary cruise through primary mission. *J. Geophys. Res. Planets*. **106**, 23429–23570 (2001), doi:10.1029/2000JE001455.
50. D. E. Smith, M. T. Zuber, H. V. Frey, J. B. Garvin, J. W. Head, D. O. Muhleman, G. H. Pettengill, R. J. Phillips, S. C. Solomon, H. J. Zwally, W. B. Banerdt, T. C. Duxbury, M. P. Golombek, F. G. Lemoine, G. A. Neumann, D. D. Rowlands, O. Aharonson, P. G. Ford, A. B. Ivanov, C. L. Johnson, P. J. McGovern, J. B. Abshire, R. S. Afzal, X. Sun, Mars Orbiter Laser Altimeter: Experiment summary after the first year of global mapping of Mars. *J. Geophys. Res. Planets*. **106**, 23689–23722 (2001), doi:10.1029/2000JE001364.

Acknowledgments:

Any use of trade, firm, or product names is for descriptive purposes only and does not imply endorsement by the U.S. Government.

This is InSight contribution 221 and LA-UR-22-27122.

We acknowledge NASA, CNES, partner agencies and institutions (UKSA, SSO, DLR, JPL, IPGP-CNRS, ETHZ, ICL, MPS-MPG), and the operators of JPL, SISMOC, MSDS, IRIS-DMC and PDS for providing SEED SEIS data. This research was carried out in part at the Jet Propulsion Laboratory, California Institute of Technology, under a contract with the National Aeronautics and Space Administration (80NM0018D0004).

Funding:

NASA-NNN12AA01C with subcontract JPL-1515835 (LVP, MCM, BC, CK, GS, DS, AV, AW).

InSight PSP grant 80NSSC20K0971 (IJD).

Funding from ETH Zurich through the ETH+ funding scheme (ETH+02 19-1: "Planet Mars") (JC, DG, SC, SCS, CD, ND, AK, GZ).

ETH research grant ETH-10 17-3 (SCS).

UK Space Agency grants ST/R002096/1, ST/V00638X/1, ST/T002026/1, ST/S001514/1 and ST/W002523/1 (AH, CC, NAT, GSC, NW, WTP).

The Australian Research Council (DP180100661 and FT210100063) (KM, AR).

This study contributes to the IdEx Université de Paris ANR-18-IDEX-0001 (PL, TK, MF, ZX, SM, CP, MP, MD).

The French Space Agency CNES and ANR fund (ANR-19-CE31-0008-08) (PL, TK, MF, XZ, EB, RG, LM, SM, CP, MP, LR, AS, AS, MD)

Center for Space and Earth Science of LANL (Student Fellow Project) (MF, CL, ER)

Author contributions:

Lead of the CTX/imaging interpretation: LVP

Lead of the SEIS interpretation: PL

Text contributions: BF, ID, GSC, JFC, LVP, PL, SCS, TK, ZX.

Edits to main text and supplementary material: BF, ID, MEB, RDL, SC, SCS.

Figures contributions: AV, BAC, CK, GS, JFC, LVP, MCM, PL, SC, TK, MF.

Data services: CP, FE.

Geological interpretation: MEB, MG, MCM.

Seismic analysis: AH, CC, CD, CP, DK, EB, GZ, JC, MD, MP, ND, PD, SC, SCS, TK, WTP.

Seismic interpretation: AH, AK, DG, DK, JC, LM, MF, PD, SM, SCS, TK, WTP, ZX.

Image analysis: AW, BAC, CMD, CK, DS, GS, ID, LVP, MCM.
Targeting orbital assets: AW, CD, DS, GS, IJD, LVP.
Seismic moment analysis: PL, TK, ZX.
Impact model contribution and/or simulations: AR, CL, GSC, KM, NW, RDL.
Seismo-atmosphere coupling work: AS, LR, MR, PL, TK.
Seismic source modeling discussion: CL, ER, MF, NAT, PL
Seismic efficiency analysis: AS, NAT.
Search for atmospheric signals: AS, PL, RFG.
InSight mission management: WBB, MPP.
SEIS instrument development and management: PL, DG, WTP, WBB.
CTX/MARCI development: MCM.
CTX/MARCI management: LVP.

Competing interests: Authors declare that they have no competing interests.

Data and materials availability: MRO data are available from the NASA-PDS repository. The InSight event catalog and waveform data are available from the IRIS-DMC, NASA-PDS, SEIS-InSight data portal and IPGP data center.

Supplementary Materials

Materials and Methods

Supplementary Text

Tables S1 and S2

Figs. S1 to S10

Figures

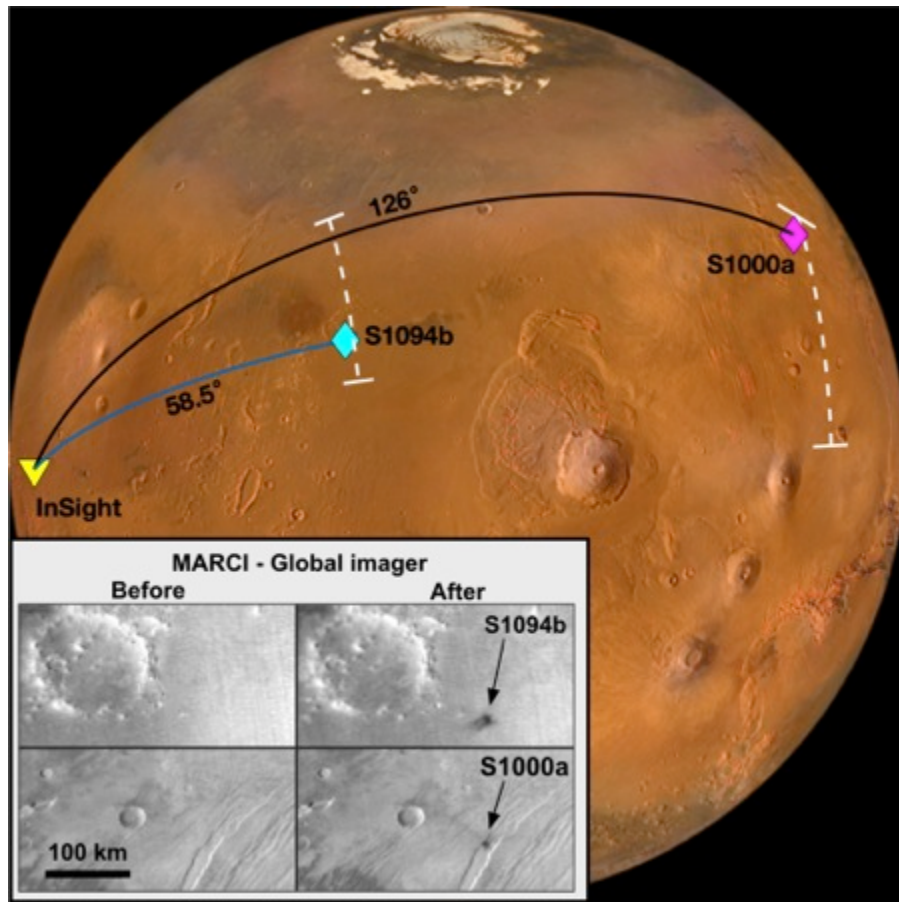


Fig. 1. Impact Event Location Map. The location of the impact craters (diamonds) and the InSight lander (yellow triangle) are shown. The S1094b crater is located at 34.80°N, 189.92°E. The S1000a crater is located at 38.11°N, 280.12°E. The great-circle paths between the new craters and InSight are superimposed onto the underlying globe image derived from MARCI (13), Mars Orbiter Camera (49) and Mars Orbiter Laser Altimeter data (MOLA) (50). The seismic epicentral distance estimates are indicated by the white-dashed lines that extend over the azimuthal uncertainty estimate. The inset shows MARCI images from before and after the impacts. The MARCI images have ~2 km/pixel resolution at nadir.

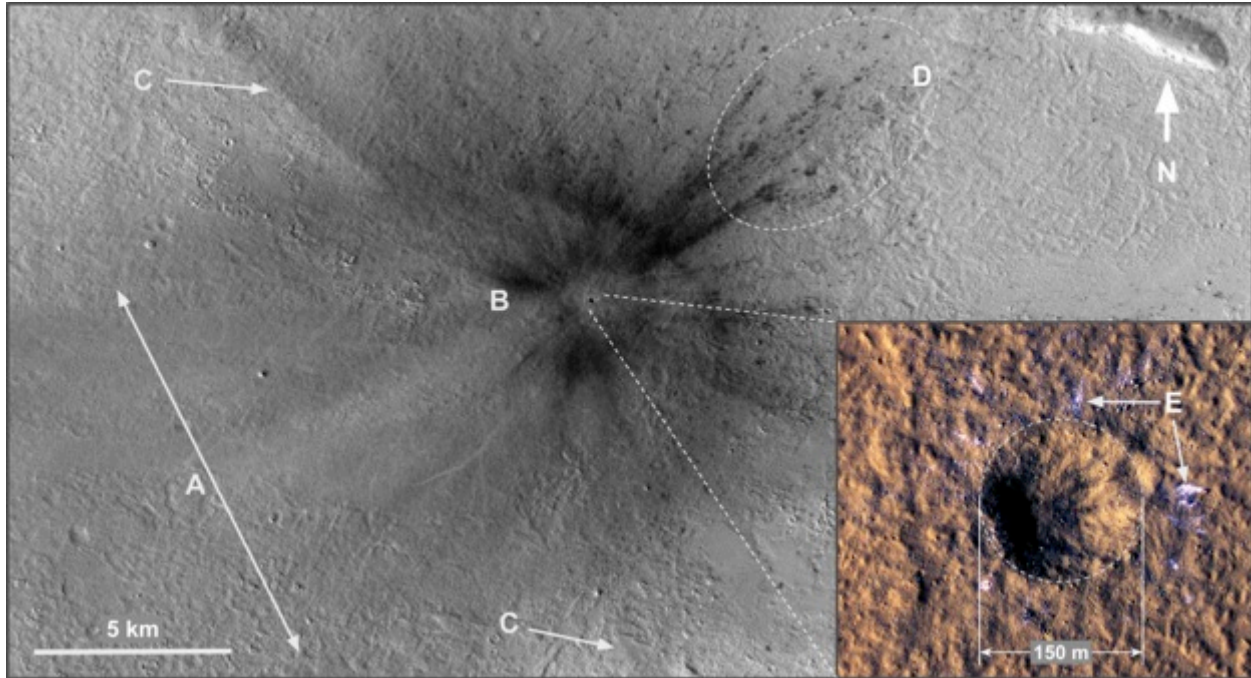


Fig. 2. Orbital images of the impact crater and surrounding area. CTX image (*main panel*): The hypervelocity impactor traveled from SW to NE at an inferred azimuth of $\sim 60^\circ$ (Fig. S3) creating a Mach cone shockwave that altered the surface albedo up-range of the impact, region A in the figure. The inner dark ring, near B, is interpreted to be the result of blast wave mobilization of surface fines, impact derived material directly deposited on the surface, or by ejecta induced disturbances of the surface dust. The absence of up-range ejecta disturbances indicates an oblique ($\sim 30^\circ$ elevation) impact (15). Faint arcuate rays, C, emanating cross-track of the impactor were likely caused by the superposition of the Mach cone and the atmospheric blast (17) indicating both blast waves propagated out at least 18 km. The long-range ejecta induced disturbances are concentrated in the down-range direction, region D, extending to at least 37 km. HiRISE image (*inset panel*): The crater has a rim-to-rim diameter of approximately 150 meters. The crater floor has an irregular shape with a depth of roughly 21 meters. The light-toned material, e.g. areas indicated by arrows E, around the crater is inferred to be water ice ejected during the impact.

CTX Image ID U05_073077_2154_XI_35N170W. Credit: NASA/JPL-Caltech/MSSS.

HiRISE Image ID ESP_073077_2155. Credit: NASA/JPL-Caltech/University of Arizona.

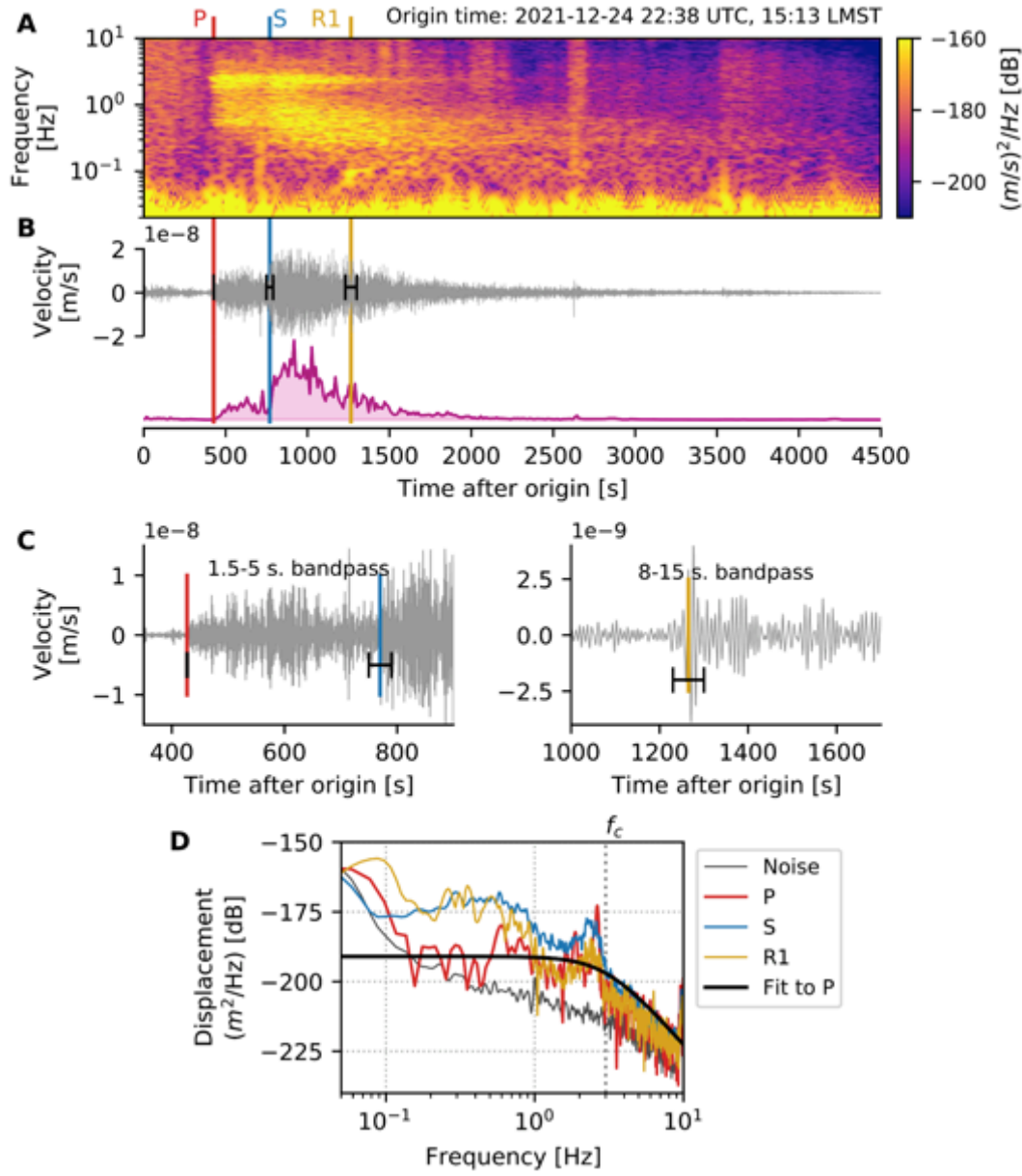


Fig. 3. Seismic observation of S1094b, using de-glitched broadband data. (A) Vertical component velocity spectrogram. The event occurs at the end of a noisy period typical of martian afternoons. (B) Vertical component velocity time series bandpassed between 1-10 sec and derived spectral envelope. Phase picks for P, S, and Rayleigh (R1) wave arrivals are indicated with pick uncertainty indicated by black bars in the timeseries. (C) Waveform details of the P and S body waves (left) and Rayleigh wave (right). (D) Displacement spectra for the P, S, and Rayleigh waves and pre-event noise. See Fig. S1 for a similar analysis of S1000a.

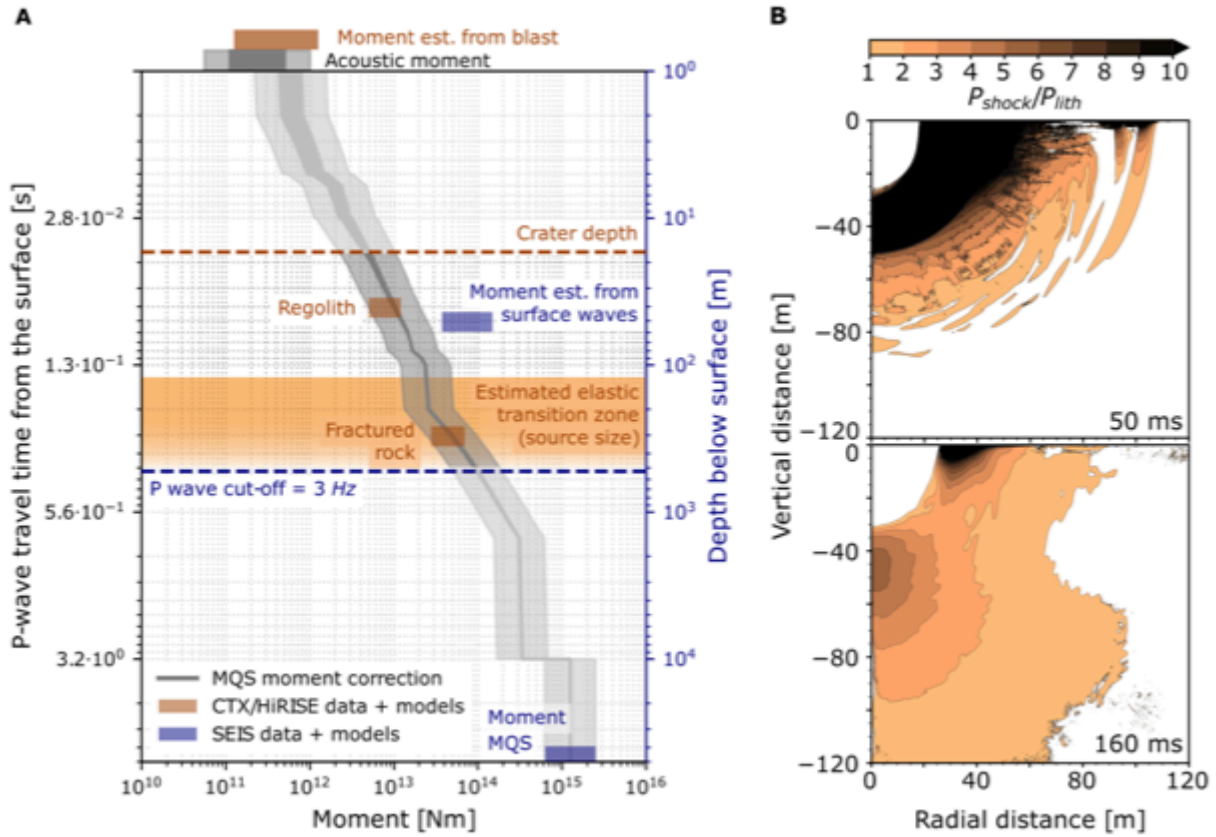


Fig. 4. Seismic source analysis for impact S1094b. (A) Seismic moment extrapolated to different source depths and in the air (gray). The blue bars are MQS moment and moment from surface wave amplitude. See more in Fig. S5 and seismic modeling methods Fig. S6. The brown bars show three moment calculations: two seismic moments estimated from crater size assuming different target materials (29, 30) and one acoustic moment at the surface. Note the overlap between the predicted moment from the atmospheric blast and the estimated acoustic moment (brown and gray bars at top of 4A). The orange-shaded region indicates the estimated depth range for the transition from shock to elastic waves (29). (B) iSALE-2D hydrocode simulation of shock wave caused by a vertical impact at 12 km/s of a 5-m-diameter (180 ton) meteoroid into fractured basalt. Two snapshots at 50 and 160 ms show the zone of seismic wave generation where the shock pressure (P_{shock}) is substantially higher than the lithostatic pressure (P_{lith}).